Electron transport properties of bilayer graphene

X. Li, K. M. Borysenko, M. Buongiorno Nardelli, and K. W. Kim

Electron Transport Properties of Bilayer Graphene

X. Li,[1] K. M. Borysenko,[1] M. Buongiorno Nardelli,[2, 3] and K. W. Kim[1, *]

[1]*Department of Electrical and Computer Engineering,*
North Carolina State University, Raleigh, NC 27695-7911
[2]*Department of Physics, North Carolina State University, Raleigh, NC 27695-8202*
[3]*CSMD, Oak Ridge National Laboratory, Oak Ridge, TN 37831*

Electron transport in bilayer graphene is studied by using a first principles analysis and the Monte Carlo simulation under conditions relevant to potential applications. While the intrinsic properties are found to be much less desirable in bilayer than in monolayer graphene, with significantly reduced mobilities and saturation velocities, the calculation also reveals a dominant influence of extrinsic factors such as the substrate and impurities. Accordingly, the difference between two graphene forms are more muted in realistic settings although the velocity-field characteristics remain substantially lower in the bilayer. When bilayer graphene is subject to an interlayer bias, the resulting changes in the energy dispersion lead to stronger electron scattering at the bottom of the conduction band. The mobility decreases significantly with the size of the generated bandgap, whereas the saturation velocity remains largely unaffected.

I. INTRODUCTION

Graphene has received much attention in the last few years due to its unique properties. In addition to the significant interests in fundamental physics, stemming in part from the relativistic-like behavior of the massless charge particles around the Dirac cone, this material is very attractive in many applications, particularly in high speed devices.[1–4] However, the gapless spectrum of monolayer graphene (MLG) makes it difficult to turn off the electrical current due to tunneling. Bilayer graphene (BLG), on the other hand, can provide a finite band gap up to hundreds of meV, when the inversion symmetry between top and bottom layers is broken by an applied perpendicular electric field.[5–8] A current on/off ratio of about 100 was observed at room temperature,[9] offering a much needed control for nonlinear functionality. Unfortunately experimental studies have also indicated that the typical mobility of charge carriers in BLG may be substantially smaller than in MLG.[10] A recent work based on the first principles calculations has suggested that this discrepancy may start with the intrinsic transport properties, which results from substantial differences in electron-phonon coupling in these two materials.[11] Additionally, it is widely accepted that extrinsic factors such as charged impurities, disorder, and surface polar phonons (SPPs) can significantly alter carrier transport in graphene on a substrate, a most commonly used configuration.[12–14] Despite extensive research efforts, a comprehensive understanding of electron transport properties in BLG is still a work in progress.

The purpose of the present paper is to address this issue theoretically by taking advantage of a first principles analysis and the Monte Carlo simulation. Specifically, the impacts of substrate conditions and perpendicular electric fields are examined. The calculation results indicate that graphene in the bilayer form loses much of its advantage over conventional semiconductors in the low-field transport, particularly when the band structure is modified to induce non-zero energy gap. The saturation drift velocity, on the other hand, can remain relatively high. Due to the screening, electrons in BLG appear less susceptible to the interactions with remote Coulomb sources, such as SPPs and impurities on the substrates, compared to the monolayer counterparts. Below, we begin with a brief overview of the models used to estimate the relevant scattering rates.

II. RELEVANT SCATTERING MECHANISMS

The strength of the electron-phonon coupling is estimated from the first principles by using the density functional theory.[11,15] A comparative analysis reveals several qualitative differences in the intrinsic scattering of MLG and BLG. For one, MLG has six phonon branches with two carbon atoms in a unit cell, whereas these numbers double in BLG. Then, BLG may need to consider both the intraband and interband transitions due to the presence of a close second conduction band π_2^* in addition to the lowest π_1^* states. At the same time, the optical phonons in BLG appear to be a relatively weak source of interaction unlike in MLG. Ultimately, the intrinsic scattering rate in BLG is dominated by the long wave acoustic phonons (intravalley scattering). Figure 1 illustrates this general trend; only the dominant branches are shown for clarity of presentation. The nomenclature for the phonon modes can be found in Refs. 11 and 15.

In the presence of a polar substrate, the graphene electron interaction with SPPs can play a significant role as the earlier studies in MLG have illustrated comprehensively.[14,16,17] A similar treatment can be extended to BLG. By assuming that the electrons are equally distributed in the two layers of BLG, we can derive the corresponding scattering rate as

$$\frac{1}{\tau_S(\mathbf{k}_i)} = \frac{2\pi}{\hbar} \sum_{\mathbf{q}} \frac{e^2 \mathcal{F}^2}{\varepsilon(q)^2} \left[\frac{e^{-2qd} + e^{-2q(d+c)}}{2q} \right]$$
$$\times \left(n_q + \frac{1}{2} \pm \frac{1}{2} \right) |g_{\mathbf{k}_i}^{s,s'}(q)|^2 \delta(E_f - E_i \pm \hbar\omega_S), \tag{1}$$

where $q = |\mathbf{k}_f - \mathbf{k}_i|$ is the magnitude of the SPP momentum, E_f (E_i) is the final (initial) electron energy, d is the distance between the first layer and the substrate (0.4 nm), c is the interlayer distance (0.34 nm), ω_S is the SPP energy, n_q is the phonon occupation number, and $\varepsilon(q)$ is the dielectric function. Additionally, $\mathcal{F}^2 = \frac{\hbar\omega_S}{2A\varepsilon_0}(\frac{1}{\kappa_S^\infty + 1} - \frac{1}{\kappa_S^0 + 1})$ is the square of Fröhlich coupling constant, where κ_S^∞ (κ_S^0) is the high (low) frequency dielectric constant of the substrate. The term $|g_{\mathbf{k}}^{s,s'}(q)|^2 = \frac{1}{2}[1 + ss' \cos\alpha_{\mathbf{k}} \cos\alpha_{\mathbf{k+q}} + ss' \sin\alpha_{\mathbf{k}} \sin\alpha_{\mathbf{k+q}} \cos 2\theta]$ comes from the overlap of the electron wave functions of the initial and final states with the scattering angle θ;[18] s and s' are the band indices whose product is $+1$ for the intraband (for example, π_1^*-π_1^*) and -1 for the interband (π_1^*-π_2^*) transitions.[19] For intrinsic BLG, $\alpha_{\mathbf{k}} = \pi/2$ for an arbitrary $\mathbf{k}$. When an interlayer bias of u is applied, it is modified to satisfy $\tan\alpha_{\mathbf{k}} = \hbar^2 k^2/m^* u$, where m^* is the effective mass of unbiased (or intrinsic) BLG at the K or K' point.[18] For MLG, $|g_{\mathbf{k}}^{s,s'}(q)|^2 = \frac{1}{2}[1 + ss' \cos\theta]$. The specific values for the relevant substrate parameters can be found in the literature.[14,16,20] As for the remote impurity scattering, the charged impurities are assumed to be located on the surface of the substrate, in which case the scattering rate is given by

$$\frac{1}{\tau_{im}(\mathbf{k}_i)} = \frac{2\pi n_i}{A\hbar} \sum_{\mathbf{q}} \left[\frac{e^2}{2\varepsilon_0 \kappa \varepsilon(q) q} \right]^2 \left[\frac{e^{-2qd} + e^{-2q(d+c)}}{2} \right]$$
$$\times |g_{\mathbf{k}}^{s,s'}(q)|^2 \delta(E_f - E_i), \tag{2}$$

where $\kappa = (\kappa_S^0 + 1)/2$ is the background dielectric constant and n_i is the impurity concentration. The other parameters are the same as defined in Eq. (1).

In the random phase approximation, the graphene dielectric function can be expressed as[18,21] $\varepsilon(q) = 1 - v_q \Pi(q)$ with the bare Coulomb interaction $v_q = e^2/2\varepsilon_0 q$ and the electron-hole propagator

$$\Pi(q) = 2 \sum_{s,s',\mathbf{k}} |g_{\mathbf{k}}^{s,s'}(q)|^2 \frac{f_{\mathbf{k+q}}^{s'} - f_{\mathbf{k}}^s}{E_{\mathbf{k+q}}^{s'} - E_{\mathbf{k}}^s}. \tag{3}$$

Here, $f_{\mathbf{k}}^s$ is the electron distribution function in band s and the factor of 2 takes into account the spin degeneracy. Figure 2 shows the numerically obtained propagators for MLG and BLG with the graphene electron density of $n = 5 \times 10^{11}$ cm^{-2} at 300 K. In this calculation [i.e., $\Pi(q)$], electron occupation in the π_2^* states is ignored for its negligible contribution. Compared to MLG, the screening in BLG appears to be much stronger due mainly to the large density of state at the bottom of the conduction band (π_1^*).[21] Additionally, the impact of the interlayer potential on the electron screening in BLG can be substantial and is a strong function of temperature.

III. ELECTRON TRANSPORT IN BLG VS. MLG

A full-band ensemble Monte Carlo calculation is used for evaluating electron transport characteristics self-consistently. The model takes into account the complete electron and phonon spectra in the first Brillouin zone. Specifically, both the graphene phonon dispersion and its interaction with electrons are obtained from the *first principles* calculations as discussed above,[11,15] whereas analytical expressions from the tight binding approximation are used for the electronic energy bands in MLG and BLG (with the nearest-neighbor hopping energy $\gamma_0 = 3.3$ eV and the interlayer hopping energy $\gamma_1 = 0.4$ eV).[22] The effect of degeneracy in the electronic system is taken into account by the rejection technique, after the final state selection. Electron scattering with the SPPs and remote impurities are also considered in the calculation as described above whenever necessary. Throughout the calculation, we assume an electron density $n = 5 \times 10^{11}$ cm^{-2} and $T = 300$ K.

Figure 3 shows the electron drift velocity as a function of the electric field in MLG and BLG (with no interlayer bias). It provides a comparison of all examined cases: namely, intrinsic graphene and graphene on two different

substrates, SiO_2 and hexagonal BN (h-BN), for which a charged impurity density of $n_i = 5 \times 10^{11}$ cm^{-2} is considered along with the SPPs. As illustrated, intrinsic MLG (i.e., no substrate) shows remarkable transport properties,[17,23] with the mobility and the saturation velocity as high as 1.0×10^6 cm^2/Vs and 4.3×10^7 cm/s. An analogous calculation for BLG gives a substantially lower mobility of 1.2×10^5 cm^2/Vs and the saturation velocity of 1.8×10^7 cm/s. These results for the intrinsic drift velocity are consistent with the scattering rates in Fig. 1; they demonstrate how acoustic and optical phonons affect the charge carriers in MLG and BLG at various electric fields.

The lower mobility in BLG can be readily explained by the larger acoustic phonon scattering rates, as well as the lower electron group velocity near the bottom of the conduction band, where all electrons tend to congregate at low electric fields. To understand the smaller saturation velocity in BLG, on the other hand, it is convenient to examine the distribution function at high electric field plotted in Fig. 4. As the electrons gain energy in the applied field, the distribution function shifts in the k-space along the direction of the drift. At the same time, increased scattering with the long-wave acoustic phonons leads to a further broadening of the electron distribution. The result of this interplay between the displacement and the broadening is the saturation of the drift velocity in intrinsic BLG, where the acoustic phonons dominate the scattering (particularly, momentum relaxation). In MLG, however, the velocity curve appears to demonstrate another pattern, which points to the presence of a competing intrinsic scatterer. Indeed, as we discussed earlier, the inelastic scattering via optical phonons is strong unlike in BLG, providing efficient energy relaxation for hot electrons. Consequently, the distribution in MLG is prevented from shifting further towards higher energies, which in turn effectively curtails the momentum relaxing interactions and results in a higher saturation velocity. Unlike in the conventional semiconductors, the loss of electron energy does not bring about the reduced group velocity (i.e., the slope) due to the linear dispersion.

A similar consideration applies when an additional source of optical phonon scattering comes into play. That is, the saturation velocity may be actually enhanced when graphene electrons are subject to the SPP scattering, as it provides another path for hot electron energy relaxation. Moreover, the SPPs prefer small angle interactions (i.e., small momentum relaxation) due to their Coulombic nature. Figure 3 clearly demonstrates this effect. In MLG, the SPP scattering can increase the saturation velocity up to 6.5×10^7 cm/s if SiO_2 or h-BN is used for the substrate material. A similar, positive impact of the substrate on the saturation velocity was also suggested in recent studies.[17,20,24] In BLG, the saturation velocity can reach 2.9×10^7 cm/s, which is about as 1.5 times large as the intrinsic value. Apparently, the enhancement of drift velocity is still prominent despite the stronger screening in BLG leading to smaller SPP scattering rates. This is due partly to the fact that the competing relaxation mechanism (i.e., intrinsic optical phonon scattering) is relatively weak in BLG as discussed earlier. Nonetheless, interactions with optical phonons (both intrinsic and SPP) provide the dominant energy relaxation process even in BLG; other mechanisms not included in the current study such as emission of photons[25] are not expected to play a significant role in the field range under consideration.

When the charged impurity scattering is taken in account, the electron drift velocities in MLG and BLG are substantially reduced at low electric fields (see Fig. 3). If h-BN is used as the substrate, the low-field mobility is 1.9×10^4 cm^2/Vs in MLG, and 1.2×10^4 cm^2/Vs in BLG. The drift velocity at the electric field of 20 kV/cm in MLG decreases to 4.8×10^7 cm/s, while in BLG it stays nearly the same as the case without impurity scattering, 2.8×10^7 cm/s. Clearly, the impact of ionized impurity scattering is much less severe in BLG. It is because the BLG electrons on average are more separated from the impurities (i.e., the surface of the substrate) and experience stronger screening. A similar trend is observed in the calculation with SiO_2 as well. In this case, the result for MLG also appears to be in good agreement with the available experimental data;[24] the discrepancy may be attributed to the presence of additional sources of interaction such as neutral scatters on the substrate, ripples and other defects in graphene crystal lattice.[4] On a related note, it is important to point out that the samples of graphene on h-BN frequently show much higher mobility measurements than those on SiO_2. This is because the graphene/h-BN interface tends to be naturally of higher quality due to their structural similarity (for example, no dangling bonds). Consequently, one can expect fewer surface impurities/defects, better stability, and reduced roughness (than graphene on SiO_2), leading to superior transport characteristics.[26] However, the interface quality varies from sample to sample, making a meaningful comparison rather difficult as it requires a thorough characterization of each interface. Our calculations, on the other hand, assume an identical impurity concentration on both substrates to elucidate the fundamental impact of this scattering mechanism in a direct one-to-one analysis.

IV.   TRANSPORT IN BLG WITH INTERLAYER BIAS

BLG with an interlayer bias offers the advantage of a tunable bandgap with potential applications to transistors, tunable photo-detectors and lasers.[6,9] The band structure in this case changes to,[5]

$$E_k^2 = \frac{\gamma_1^2}{2} + \frac{u^2}{4} + \hbar^2 v_F^2 k^2 \pm \sqrt{\frac{\gamma_1^4}{4} + \hbar^2 v_F^2 k^2 (\gamma_1^2 + u^2)}, \tag{4}$$

where u is the difference between on-site energies in the two layers, $v_F = (\sqrt{3}/2) a \gamma_0 / \hbar \approx 1 \times 10^8$ cm/s is the Fermi velocity ($a = 0.246$ nm), and the minus and plus signs correspond the π_1^* and π_2^* conduction bands, respectively. However, this ability to tune the band gap comes at the expense of the material's intrinsic transport properties. As the bandgap opens, the bottom of the lowest conduction band changes its shape from a hyperbola to a so-called "Mexican hat" and the density of states exhibits a Van Hove singularity as shown in Fig. 5. Consequently, the increased density of states leads to stronger quasi-elastic electron interaction with the long-wavelength acoustic phonons at low electron energies. Figure 6 provides the dependence of the mobility on the size of the bandgap. When the bandgap reaches 0.24 eV, the mobility drops to as low as 1.2×10^4 cm^2/Vs even without any external scattering mechanisms, which is one order of magnitude smaller than in the unbiased case. The reduction in the mobility becomes even more pronounced when the ionized impurity scattering is taken into account. The Van Hove singularity also enhances the impact of electron coupling with the remote impurities.

On the other hand, it appears that the velocities at high fields are mostly unaffected by the gap. Figure 7 shows the drift velocity for $u = 0.1$ V, 0.2 V, and 0.3 V, which correspond to the bandgap of 0.1 eV, 0.18 eV, and 0.24 eV, respectively. As the phenomenon of velocity saturation is associated with hot electrons, it is relatively immune from the changes at the bottom of the energy dispersion. Similarly, the impact of the SPP scattering on the drift velocity, as it is felt primarily via the high energy electrons, is not affected by the gap in the electron energy spectrum. Accordingly, no appreciable difference is observed in the saturation velocities for the three considered values of u. When the ionized impurity scattering is included, the velocity saturation is progressively pushed to a higher field due to the reduction in the mobility (i.e., the slope) that was discussed above.

Finally, it may be worth pointing out that the electron-electron scattering could potentially be significant for accurate calculation of low-field transport properties in biased BLG. Due to the diverging density of states at the band minima, electrons tend to congregate in the low-energy states with small momentum vectors, causing stronger inter-carrier interactions. Accordingly, it could limit the accuracy of the obtained mobility values even at the assumed relatively low density of 5×10^{11} cm^{-3}. This is not a concern in MLG or BLG without the interlayer bias as their density of states is finite even at zero energy.

V.   SUMMARY

Electron transport properties of BLG are studied under realistic conditions in the presence of the SPPs and charged impurities. Overall, BLG has a lower mobility and saturation velocity than MLG, due to the stronger acoustic phonon scattering, weaker optical phonon scattering, and nonlinear dispersion at the bottom of the conduction band. It is also shown that SPPs can improve the saturation velocity in BLG by effectively dissipating the electron energy. The impurity scattering has a considerable effect in decreasing the drift velocities in both MLG and BLG. However, BLG appears more resistant to impurity scattering than MLG, due to a stronger screening and larger effective distance between electrons and the impurities. In BLG with a interlayer bias, the changes in the band structure result in drastically reduced mobilities, particularly in the presence of charged impurities. This may have a negative consequence in the potential device application.

Acknowledgments

* Electronic address: kwk@ncsu.edu

[1] K. S. Novoselov, A. K. Geim, S. V. Morozov, D. Jiang, Y. Zhang, S. V. Dubonos, I. V. Grigorieva, and A. A. Firsov, Science **306**, 666 (2004).

[2] K. S. Novoselov, A. K. Geim, S. V. Morozov, D. Jiang, M. I. Katsnelson, I. V. Grigorieva, S. V. Dubonos, and A. A. Firsov, Nature **438**, 197 (2005).

[3] Y.-M. Lin, C. Dimitrakopoulos, K. A. Jenkins, D. B. Farmer, H.-Y. Chiu, A. Grill, and Ph. Avouris, Science **327**, 662 (2010).

[4] A. H. Castro Neto, F. Guinea, N. M. R. Peres, K. S. Novoselov, and A. K. Geim, Rev. Mod. Phys. **81**, 109 (2009).

[5] E. McCann, Phys. Rev. B **74** 161403(R) (2006).

[6] E. V. Castro, K. S. Novoselov, S. V. Morozov, N. M. R. Peres, J. M. B. Lopes dos Santos, J. Nilsson, F. Guinea, A. K. Geim, and A. H. Castro Neto, Phys. Rev. Lett. **99**, 216802 (2007).

[7] H. Min, B. Sahu, S. K. Banerjee, and A. H. MacDonald, Phys. Rev. B **75**, 155115 (2007).

[8] Y. Zhang, T. Tang, C. Girit, Z. Hao, M. C. Martin, A. Zettl, M. F. Crommie, Y. R. Shen, and F. Wang, Nature, **459**, 820 (2009).

[9] F. Xia, D. B. Farmer, Y.-M. Lin, and Ph. Avouris, Nano Lett. **10**, 715 (2010).

[10] S. Xiao, J.-H. Chen, S. Adam, E. D. Williams, and M. S. Fuhrer, Phys. Rev. B **82**, 041406(R) (2010).

[11] K. M. Borysenko, J. T. Mullen, X. Li, Y. G. Semenov, J. M. Zavada, M. Buongiorno Nardelli, and K. W. Kim, Phys. Rev. B **83**, 161402(R) (2011).

[12] C. Jang, S. Adam, J.-H. Chen, E. D. Williams, S. Das Sarma, and M. S. Fuhrer, Phys. Rev. Lett. **101**, 146805 (2008).

[13] S. Das Sarma, E. H. Hwang, and E. Rossi, Phys. Rev. B **81**, 161407(R) (2010).

[14] S. Fratini and F. Guinea, Phys. Rev. B **77**, 195415 (2008).

[15] K. M. Borysenko, J. T. Mullen, E. A. Barry, S. Paul, Y. G. Semenov, J. M. Zavada, M. Buongiorno Nardelli, and K. W. Kim, Phys. Rev. B **81**, 121412(R) (2010).

[16] A. Konar, T. Fang, and D. Jena, Phys. Rev. B **82**, 115452 (2010).

[17] X. Li, E. A. Barry, J. M. Zavada, M. Buongiorno Nardelli, and K. W. Kim, Appl. Phys. Lett. **97**, 232105 (2010).

[18] X. F. Wang and T. Chakraborty, Phys. Rev. B **81**, 081402(R) (2010).

[19] This expression for $g_{\mathbf{k}}^{s,s}(q)$ is also applied to the π_2^*-π_2^* scattering even though it is only approximate. the treatment does not alter the calculation results due to the small contribution of the electrons in the π_2^* band.

[20] V. Perebeinos and Ph. Avouris, Phys. Rev. B **81**, 195442 (2010).

[21] E. H. Hwang and S. Das Sarma, Phys. Rev. Lett. **101**, 156802 (2008).

[22] Z. Q. Li, E. A. Henriksen, Z. Jiang, Z. Hao, M. C. Martin, P. Kim, H. L. Stormer, and D. N. Basov, Phys. Rev. Lett. **102**, 037403 (2009).

[23] X. Li, E. A. Barry, J. M. Zavada, M. Buongiorno Nardelli, and K. W. Kim, Appl. Phys. Lett. **97**, 082101 (2010).

[24] A. M. Dasilva, K. Zou, J. K. Jain, and J. Zhu, Phys. Rev. Lett. **104**, 236601 (2010).

[25] F. T. Vasko and O. G. Balev, Phys. Rev. B. **82**, 165449 (2010).

[26] R. Decker, Y. Wang, V. W. Bar, W. Regan, H. Z. Tsai, Q. Wu, W. Gannett, A. Zettl, and M. F. Crommie, Nano Lett. **11**, 2291 (2011).

Figures

FIG. 1: (Color online) Intrinsic electron scattering rates in MLG and BLG calculated from the first principles for the dominant (a) acoustic and (b) optical phonons.[11,15] The sudden increases shown in (b) are due to the onset of optical phonon emission. They correspond to the phonon frequencies at the points of high symmetry in the first Brillouin zone: $\omega_\Gamma \approx 200$ meV and $\omega_K \approx 160$ meV.

FIG. 2: (Color online) Electron-hole propagator $\Pi(q)$ normalized to N_0 ($= 2m^*/\pi\hbar^2$) in MLG and BLG with the graphene electron density of 5×10^{11} cm^{-2}. For BLG, the calculation considers different interlayer biases with the induced energy gap E_g of 0 eV (no bias), 0.10 eV, 0.18 eV, and 0.24 eV, respectively.

FIG. 3: (Color online) Electron drift velocity versus electric field in (a) MLG and (b) BLG, with different substrate conditions: intrinsic/no substrate (circle), SiO$_2$ (triangle), SiO$_2$ with impurities (reverse triangle), h-BN (square), and h-BN with impurities (diamond). The electron density is 5×10^{11} cm^{-2} at 300 K. The impurities on the surface of the substrate (d=0.4 nm) have the density 5×10^{11} cm^{-2}.

FIG. 4: (Color online) Cross sectional view (k_y=0) of electron distribution functions in (a) MLG and (b) BLG at 20 kV/cm, with different substrate conditions: intrinsic/no substrate (short dashed line), SiO$_2$ (long dashed line), SiO$_2$ with impurities (solid line), h-BN (dashed-dotted line), and h-BN with impurities (dotted line). The conditions are the same as specified in Fig. 3.

FIG. 5: (Color online) Density of states in BLG for different interlayer biases with the induced energy gap E_g of 0 eV (solid line), 0.10 eV (dashed line), 0.18 eV (dotted line), and 0.24 eV (dashed-dotted line), respectively. The inset shows the corresponding band structures.

FIG. 6: (Color online) Electron mobility versus bias-induced bandgap in BLG at 300 K, with different substrate conditions. The electron density is 5×10^{11} cm^{-2}. The impurities on the surface of the substrate (d=0.4 nm) have the density 5×10^{11} cm^{-2}.

FIG. 7: (Color online) Electron drift velocity versus electric field in BLG with a bias-induced gap of E_g of (a) 0.1 eV, (b) 0.18 eV, and (c) 0.24 eV, under different substrate conditions: intrinsic/no substrate (circle), SiO$_2$ (triangle), SiO$_2$ with impurities (reverse triangle), h-BN (square), and h-BN with impurities (diamond). The conditions are the same as specified in Fig. 6.
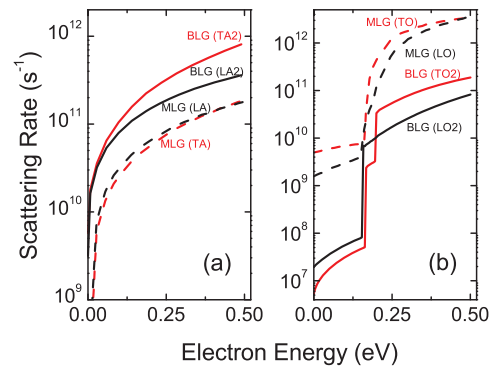
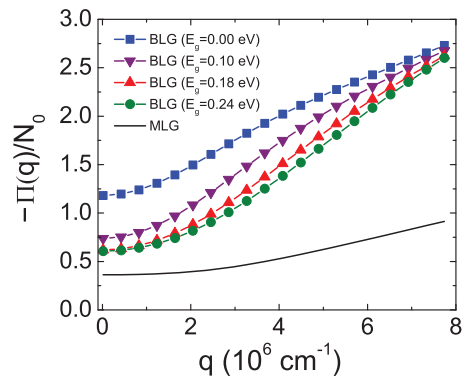Figure 1   BJ11837   09Nov2011

Figure 2   BJ11837   09Nov2011
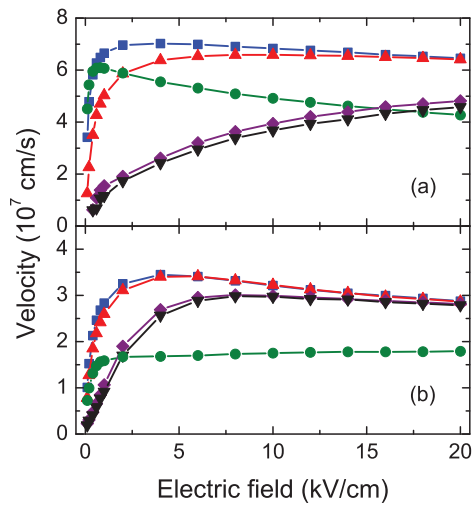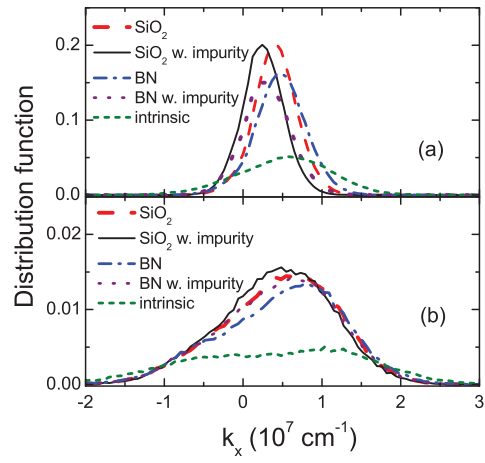
Figure 3   BJ11837   09Nov2011

Figure 4   BJ11837   09Nov2011
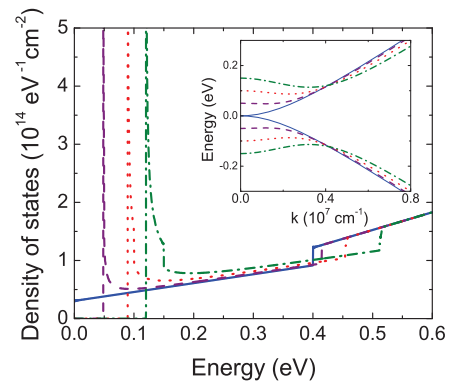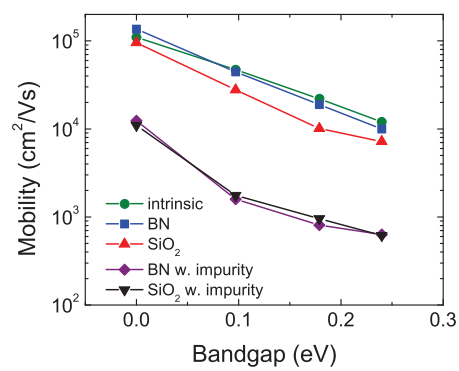
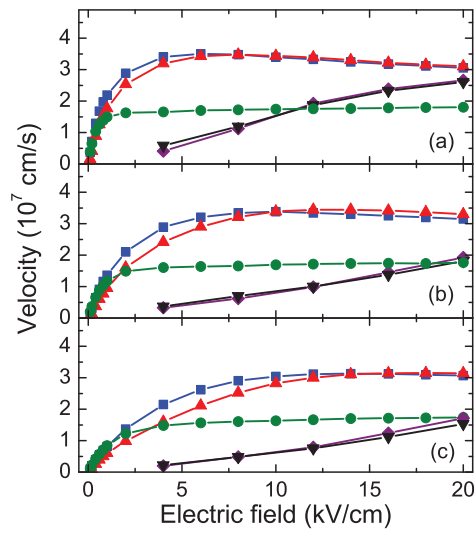Figure 5   BJ11837   09Nov2011

Figure 6   BJ11837   09Nov2011

Figure 7   BJ11837   09Nov2011